Maximizing the Data Rate of an Inductively Coupled Chip-to-Chip Link by Resetting the Channel State Variables

Nagendra Krishnapura, *Member, IEEE*, Anoop Narayan Bhat, Subhashish Mukherjee, Kumar Anurag Shrivastava, and Madhulatha Bonu

***Abstract*— A technique is proposed for increasing the data rate transmitted through an inductively coupled chip-to-chip link by resetting the channel state variables. This allows the data rate to be increased well beyond what is implied by the channel bandwidth. In the proposed scheme, the two sides of the link are resonated at the highest possible quality factor, maximizing link gain, and minimizing interference. The transmit signal is a binary matched pulse which maximizes the received signal for a given transmitter voltage limit. High-efficiency switching transmitters can be used for this type of signal. The proposed technique can be applied to communication links in which channel state variables are accessible for reset. For increasing the data rate, it is shown that the proposed state-variable reset technique results in a higher signal-to-noise ratio of the received signal and a higher energy efficiency compared to reducing the quality factor to widen the bandwidth, using equalization, or using multi-level signaling. The technique is demonstrated on a chip-to-chip link with coupled 1.5 mm × 1.5 mm planar inductors separated by 0.5 mm in a 0.18μm CMOS process. 500 Mb/s data rate is achieved over a link which has a band-pass bandwidth of 185 MHz.**

***Index Terms*— Matched filters, time varying circuits, state-variable reset, isolator, chip-to-chip link, inductively coupled link.**

I. Introduction

INDUCTIVE near-field links are used widely for short-range data transmission. Applications include digital data transmission requiring electrical isolation [1], [2], radio frequency identification (RFID), implantable medical devices (IMDs [3]–[5]), and chip-to-chip high-bandwidth links [6]–[8]. Minimizing the power dissipated in the transmitter and receiver circuits is important, especially when a part of the circuit works from harvested energy. In high-speed links like [7], [8], the power consumed by inductively coupled links can be several watts, and a reduction can mean significant power savings. In most of the inductively coupled links in the above mentioned-applications, the coupling coefficient between inductors is rather low (< 0.1) resulting in a very small received signal. This is especially so when high voltage isolation is required between the two sides. The least expensive option for obtaining high isolation is to have large physical separation between two in-plane chips with planar inductors on each [9], [10]. In such cases, the inductive coupling coefficient k is of the order of 0.01. Therefore, for error-free data transmission, either high power has to be transmitted, or a more sensitive receiver has to be designed, both of which increase the total power consumption of the link. In this work, we investigate signaling and circuit techniques which increase the data rate and the received signal-to-noise ratio (*SNR*) as much as possible while keeping the transmitter power dissipation to be as small as possible.

One way to increase the signal gain through the channel is to resonate the two sides of the inductively coupled link at a certain frequency f_0. The steady-state gain at f_0 is proportional to Q^2, where Q is the quality factor of the two resonances. But a higher Q also means a lower bandwidth and a lower data rate. Previous work in the literature for increasing the data rate through inductively coupled links use low Q. [3] demonstrates a 2.5 Mbps through a link resonated at 7 MHz with $Q = 2.5$. [4], [5] use equalization to broaden the channel bandwidth, but the Q of one of the resonances of the inductive link has to be limited to 1. Also, the excitation is a narrow pulse, lowering the transmitted and received energy. The direct antenna modulation proposed in [11] removes the persistent sinusoidal response across the primary tank but uses a low Q secondary to avoid ringing. In the very high-speed chip-to-chip links in [7], [8], Q is very low. The coils are placed very close ($< 50\mu$m) to each other, and the received signal strength is not an issue.

In this work, we propose a new technique to increase the data rate through a high Q inductively coupled link well beyond what is implied by the link bandwidth. Narrowband channels have a long memory and a long impulse response which sets the minimum symbol period. The memory is in the state variables which are distributed over the length of the channel. But, in a resonant inductively coupled link, the state variables are the inductor current and capacitor voltage at either end of the link. As will be explained in Section III of this paper, by resetting these, the channel's impulse response can be shortened arbitrarily, allowing a higher symbol rate. The received noise variance also reduces as a result of reset. To maximize the received signal, we use

Manuscript received March 22, 2019; revised June 5, 2019; accepted June 24, 2019. Date of publication July 26, 2019; date of current version August 28, 2019. This paper was recommended by Associate Editor D. Zito. *(Corresponding author: Nagendra Krishnapura.)*

N. Krishnapura is with the Department of Electrical Engineering, IIT Madras, Chennai 600036, India (e-mail: nagendra@iitm.ac.in).

A. N. Bhat was with Texas Instruments India Pvt. Ltd., Bengaluru 560093, India. He is now with the University of Twente, 7522 NB Enschede, The Netherlands.

S. Mukherjee, K. A. Shrivastava, and M. Bonu are with Texas Instruments India Pvt. Ltd., Bengaluru 560093, India.

Color versions of one or more of the figures in this article are available online at http://ieeexplore.ieee.org.

Digital Object Identifier 10.1109/TCSI.2019.2926143

1549-8328 © 2019 IEEE. Personal use is permitted, but republication/redistribution requires IEEE permission.
See http://www.ieee.org/publications_standards/publications/rights/index.html for more information.

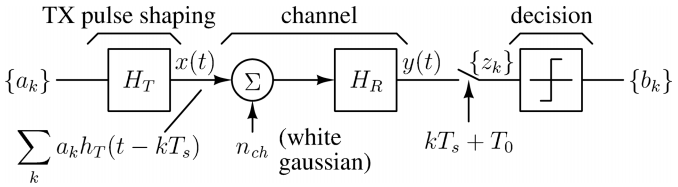

Fig. 1. Digital data $\{a_k\}$ pulse shaped by $H_T(f)$ transmitted over a channel with additive noise n_{ch} and channel response $H_R(f)$.

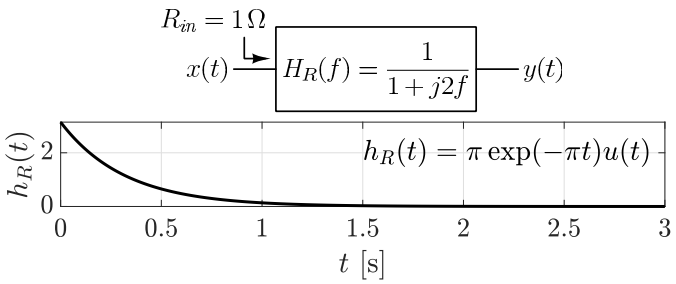

Fig. 2. First-order channel and its impulse response.

a voltage limited transmit signal matched to the channel's impulse response [12]. When the energy drawn from the transmitter power supply is considered, this technique can yield a higher efficiency (ratio of received energy to energy drawn by the transmitter) than the well known matched filter [13] approach. A prototype link based on these principles demonstrates 500 Mb/s data rate over a 185 MHz bandwidth link.

In the next section, we review data transmission through noisy channels and conditions for maximizing the received signal. In Section III, we describe the proposed state-variable reset technique. For simplicity, we use a channel with a first-order transfer function in these two sections. In Section IV, we descibe the use of this technique with the resonant inductively coupled link. We show that for any symbol period, using the binary matched transmit signal in a high Q link with reset yields a higher received signal than a low Q link which settles within the period. We also show that state-variable reset reduces noise and interference. In Section VI, we compare this with other published approaches for increasing data rate through narrowband channels. Section V describes the prototype chip. Section VII describes the measured results. Section VIII concludes the paper.

II. Data Transmission Through a Noisy Channel

In this section, we first discuss pulse transmission through a noisy channel, the *SNR* of the received signal, and maximizing the energy efficiency, defined as the ratio of the received symbol energy to the energy expended in the transmitter. Following this, we discuss the rate of data transmission through the channel, methods of increasing it, and their implication on *SNR* and efficiency.

A. SNR of the Received Signal and Energy Efficiency

Fig. 1 shows the typical model of a digital communication link [13]. Digital symbols $\{a_k\}$ are transmitted at a rate $f_s = 1/T_s$ over a noisy analog channel. The link is modeled with an additive white noise n_{ch}, a filter $H_T(f)$ preceding noise addition, and a filter $H_R(f)$ following it. In general, H_T is the combination of transmit pulse shaping, any other filtering in the transmitter, and any filtering in the channel before the noise is added. H_R is the combination of continuous-time filtering in the channel after the noise is added and receiver filtering. For simplicity, in this section, we will assume that H_R represents the channel, and H_T represents the transmit pulse shaping. $\{z_k\}$, the samples of the analog signal $y(t)$ at a period T_s (with an offset T_0 to account for delays) are sliced to obtain the received symbols $\{b_k\}$. To minimize the bit error ratio (BER), *SNR* of $y(t)$ at the sampling instants must be maximized. For low power operation, the transmitter power to obtain a given *SNR* at the receiver should be minimized.

Throughout this section, a first-order low-pass channel with a 0.5 Hz bandwidth is used as an example. Fig. 2 shows the transfer function and impulse response. The input resistance is assumed to be 1 Ω so that the square of the driving input can be interpreted as the power driven into the channel.

When a single symbol $a_0 = 1$ is transmitted, the transmitted signal is $x(t) = h_T(t)$ and the output of the channel is $h_{TR} = h_T * h_R$. The well known matched filter [13] results state that for a given transmit symbol energy, to maximize the *SNR* of the sampled received signal, H_T and H_R should be matched, i.e. $H_T(f) = H_R^*(f)$, or $h_T(t) = h_R(-t)$. The receiver sampling offset must be chosen so that the peak of h_{TR} is sampled. If h_R is fixed, matched filtering condition maximizes the peak of the received signal h_{TR} for a given energy $E_T = \int_0^\infty h_T^2(t)dt$ in the transmit pulse. In a real transmitter, to make $h_T(t)$ causal and time limited to a chosen pulse width T_w, $h_T(t) = h_R(T_w - t)$ for $0 \le t \le T_w$ and zero elsewhere.

In many practical communication links, it is not the transmit symbol energy, but the transmit peak voltage that is constrained (by the supply voltage). Assume that the transmit signal $x(t)$ is limited to ± 1 V, i.e., $|x(t)| \le 1$. $h_T(t)$ must also satisfy this constraint. With this in mind, we try to choose $h_T(t)$, confined to $0 \le t \le T_w$, such that channel output $y = \int_0^t h_T(t-\tau)h_R(\tau)d\tau$ at $t = T_w$ is maximized. This turns out to be [12]

$$h_T(t) = \begin{cases} \text{sgn}\left(h_R(T_w - t)\right), & 0 \le t < T_w \\ 0, & \text{otherwise} \end{cases} \tag{1}$$

In that case, the output is

$$y_{max}(T_w) = \int_0^{T_w} |h_R(\tau)|\, d\tau \tag{2}$$

The output is maximized since the convolution integral that yields $y(t)$ is made to have its maximum possible positive value throughout the interval, subject to the constraint $|h_T| \le 1$. Therefore, the transmit filter's impulse response has to be chosen to be binary valued, and equal to the transmitter voltage limits, according to (1). We refer to (1) as the binary matched transmit pulse.

For $h_R(t)$ shown in Fig. 2, Fig. 3(a) shows the matched pulse $h_T(t) = h_R(T_w - t)$, normalized to a peak of 1, for

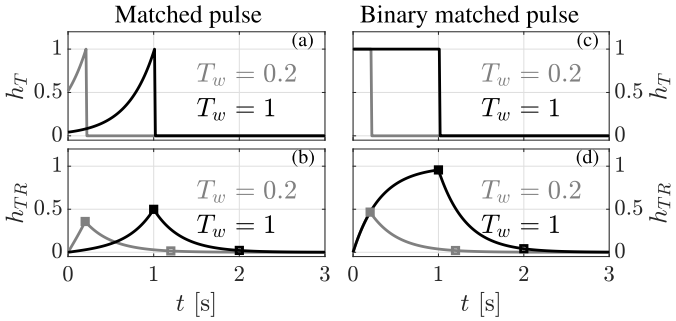

Fig. 3. (a) Transmit pulse matched to the channel in Fig. 2, (b) Corresponding channel output y, (c) Binary matched transmit pulse in (1) for the channel in Fig. 2, (d) Corresponding received signal. Shown for $T_w = 0.2$ and $T_w = 1$.

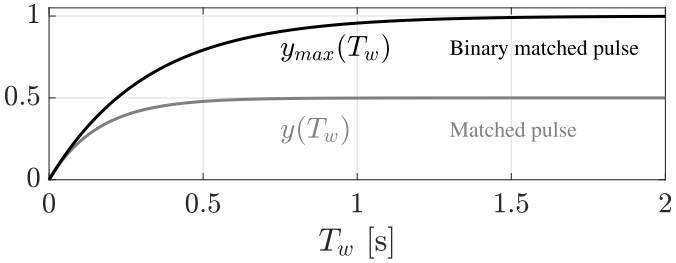

Fig. 4. Peak value of the received pulse for the first-order channel in Fig. 2.

$T_w = 0.2$ and $T_w = 1$. Fig. 3(b) shows the channel output $h_{TR} = h_T * h_R$ corresponding to these inputs. Fig. 3(c) shows the binary matched transmit pulse $h_T(t) = \text{sgn}(h_R(T_w - t))$ for $T_w = 0.2$ and $T_w = 1$. Fig. 3(d) shows the channel output $h_{TR} = h_T * h_R$ corresponding to these. It is seen that the peaks in h_{TR} are larger with a binary matched pulse. The matched filter is more "efficient" in that the energy $\int h_T^2(t)dt$, dissipated in $R_{in} = 1\ \Omega$ in Fig. 2, is smaller for a given peak value of h_{TR}, but the binary matched case provides a higher peak value because of the voltage limit on the transmit pulse h_T. Fig. 4 shows the received signal peak for the first-order channel in Fig. 2 versus truncation width T_w with the matched pulse normalized to a peak of 1 and the binary matched pulse in (1). The received signal peak saturates for large T_w in both cases but is always higher for the binary matched pulse. This shows that the binary matched pulse maximizes the received *SNR* when the transmitter is voltage limited.

The received energy E_R in case of the matched pulse and E_R' in case of the binary matched pulse are defined to be the square of the received signal peak (marked by squares in Fig. 3(b, d)) in the respective cases. The efficiency is computed as the ratio of E_R or E_R' to the energy dissipation in the transmitter. When a matched transmit pulse $h_R(T_w - t)$ is used, the energy transmitted into the (1 Ω termination of the) channel is $E_T = \int_0^{T_w} h_T^2(t)dt$. This is the smallest possible for a given received energy E_R. In practice, what is relevant is not the transmit energy E_T but the average energy drawn from the power supply for transmitting a symbol. This depends on the type of transmitter that is used. To transmit complicated pulse shapes given in Fig. 3(a) required for matched filtering, a class-A or a class-B transmitter, shown in Fig. 5(a) and (b) respectively, has to be used. In an ideal class-A transmitter, the average bias current drawn from the supplies is a constant

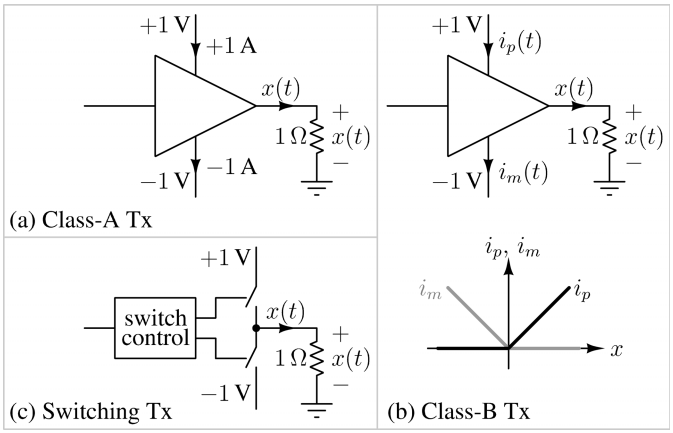

Fig. 5. (a) Class-A, (b) Class-B, (c) Switching transmitters. The 1 Ω resistor shown is the input resistance of the channel in Fig. 2.

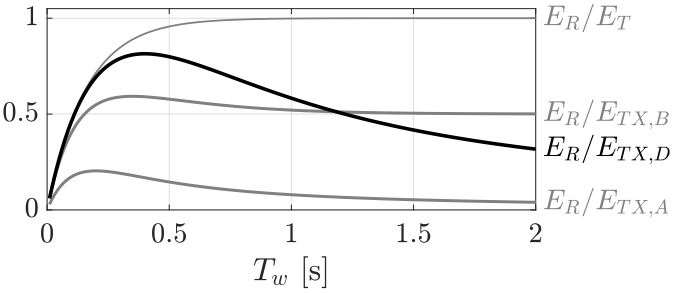

Fig. 6. Efficiency, normalized to the highest value of E_R/E_T.

and equal to the maximum load current. For transmitting h_T shown in Fig. 3(a), the average bias current is 1 A. The average energy drawn from the supply over the pulse duration is given by $E_{TX,A} = 2T_w$. In an ideal class-B transmitter, the current drawn from the positive or the negative rail equals the current pushed into or pulled out from the load respectively. In this case, the energy drawn from the supply over pulse duration is given by $E_{TX,B} = \int_0^{T_w} |h_T(t)|dt$. In either case, the energy drawn from the supply is more than the transmit energy E_T. To transmit binary matched pulses given by (2), the switching transmitter shown in Fig. 5(c) can be used. Its theoretical efficiency is 100%. In this case, the energy drawn from the supply is $E_{TX,D} = T_w$ and is the same as the energy transmitted into the channel.

Fig. 6 shows the efficiency of these approaches for the first-order channel as a function of T_w, the transmit pulse width. E_R/E_T is the ratio of the received energy to transmitted energy for the matched filter. This ratio saturates for large values of T_w because there is very little energy in h_R or h_T beyond the truncation interval T_w, and both E_R and E_T saturate. In the plot, the maximum value of E_R/E_T is normalized to unity. $E_R/E_{TX,A}$ and $E_R/E_{TX,B}$ are the ratios of the received energy to the energy drawn from the supply (over the pulse duration T_w) with ideal class-A and class-B transmitters. As expected, these are substantially lower than E_R/E_T. This ratio continuously degrades for a class-A transmitter since it continuously draws current. It saturates for a class-B transmitter since it draws very little current after the transmit pulse decays to very small values. The figure also

shows $E_R/E_{TX,D}$, the corresponding ratio with a switching transmitter (Fig. 5(c)) driving a binary matched pulse. This outperforms the matched filter with an ideal class-B transmitter for $T_w \leq 1.2$. For higher values of T_w, the received symbol energy saturates, but the switching transmitter still draws a current continuously. But, as seen later, such large values of T_w are not used since it restricts the symbol rate. Also, in practice, there will be more energy overheads in implementing a matched filter pulse and the efficiency of class-A and class-B transmitters will be significantly worse than what is seen in Fig. 6. For these reasons, the binary matched pulse is usually the most energy efficient choice for communication links in which the transmitter voltage is limited. This is confirmed by the widespread use of rectangular pulses for data transmission through low-pass channels whose impulse response h_R is usually always positive. In the rest of this paper, we consider a switching transmitter with a ± 1 V supply and a binary matched transmit pulse. The effect of the data transmission rate on the received *SNR* is considered next.

B. Data Rate and Its Effect on the Received SNR

1) Binary Signaling: In this case the symbols a_k in Fig. 1 are ± 1. With 0.5 Hz channel bandwidth, 1 bit per second (b/s) is chosen as the symbol rate. The intersymbol interference (ISI) is about 27 dB below the peak sample value. Increasing the data rate beyond this increases the ISI and reduces the worst case amplitude at the sampling instant (i.e., the eye-opening). The interfering samples are shown using markers in Fig. 3(b, d). In what follows, binary transmission at 1 b/s through this channel will be used as the baseline for comparisons. To keep transmit pulses confined to one period, we have to use $T_w \leq T_s$. We choose $T_w = T_s$ so that the received symbol energy is as large as possible (Fig. 4).

2) Multi-level Signaling: The number of bits per symbol, and therefore, the bit rate, can be increased using multi-level signaling at the same symbol rate. For N level signaling, assuming even N and limits of ± 1, the symbols a_k in Fig. 1 are $\pm 1/(N-1), \pm 3/(N-1), \ldots, \pm 1$. There are $\log_2 N$ bits per symbol. An ideal switching transmitter whose supply voltage varies according to the symbol to be transmitted is assumed. For a given noise level, the BER is higher than with binary transmission since the minimum symbol separation, and, therefore, the *SNR*, is $1/(N-1)$ times smaller. ISI is proportional to symbol amplitude. The worst case ISI occurs when the interfering symbol is 1, and the current symbol is $1/(N-1)$. Relative to the current symbol, this is $N-1$ times more than with binary transmission. This forces a lower data rate, but we ignore this and assume the same symbol rate as for binary transmission. Since the symbol values are less than or equal to those in the binary case, the average energy transmitted is lower. Assuming equal probability for all symbols, the average energy per symbol is $(N+1)/3(N-1)$ and the average energy per bit is $(N+1)/3(N-1)\log_2 N$ [13].

3) Equalization: Another option to increase the bit rate is to use an equalizer in the receiver to widen the bandwidth and increase the symbol rate in the same proportion. For the first-order channel in Fig. 2, we can use a pole-zero equalizer with transfer function $H_{eq} = (1+j2f)/(1+jf/f_1)$ in the receiver. The overall response $H_R H_{eq}$ will be a first-order filter of bandwidth f_1. Both data rate and noise variance increase by a factor $f_1/0.5$. The received signal amplitude is not affected since the bandwidth and data rate increase in the same proportion. *SNR* is lower by a factor $f_1/0.5$ and BER is higher compared to the original case due to increased noise.

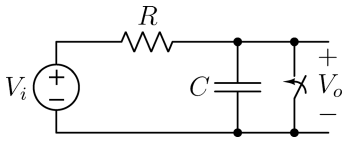

Fig. 7. Resetting the state variables of a filter.

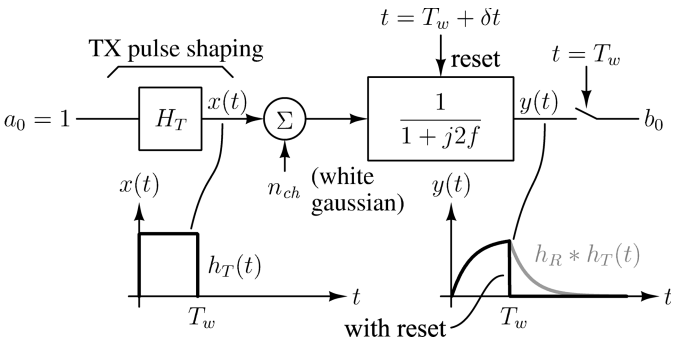

Fig. 8. Driving a pulse through a first-order channel with reset.

III. Increasing the Data Rate by Resetting the Channel State Variables

As mentioned before, to increase the data rate, the impulse response h_R of the channel has to be shortened. The channel is a continuous-time filter of some sort. We propose to truncate such a filter's response by forcing all its state variables to zero at a certain instant. Fig. 7 shows an example in which the capacitor voltage is forced to zero by short-circuiting its terminals. If there are inductors, they have to be open circuited. Usually, a channel is a distributed system (e.g. a cable or a transmission line on a PCB), and its state variables are not accessible. In a chip-to-chip link, however, the memory of the channel is in the inductors and capacitors in the transmitter and receiver, and is therefore accessible for reset.

Fig. 8 shows a 0.5 Hz bandwidth first-order low-pass channel defined in Fig. 2 driven by the binary matched pulse $h_T(t)$ defined in (1). A single symbol $a_0 = 1$ is input the transmitter. In absence of reset, the receiver's output would be $y(t) = h_T(t) * h_R(t)$. This is shown in gray. Suppose that the channel's state variables are reset just after sampling $y(t)$ at $t = T_w$. Then the output falls to zero at $t = T_w$, as shown in Fig. 8. The output would be reset to zero, as shown in Fig. 8. If another pulse is launched after this, its response will be exactly identical to the first one since the filter (channel) starts from a reset state. Thus, symbols can be transmitted with a period of $T_s \geq T_w$ with zero ISI. The peak of the received signal, which is the signal amplitude at the sampling instant $t = T_w$, is $\int_0^{T_w} |h_R(t)|dt$, is exactly the same as in (2). To maximize the data rate, the system is operated with $T_s = T_w$. This system requires the reset signal to be generated just after sampling the output. Details of its implementation for the inductively coupled link will be discussed in Section V.

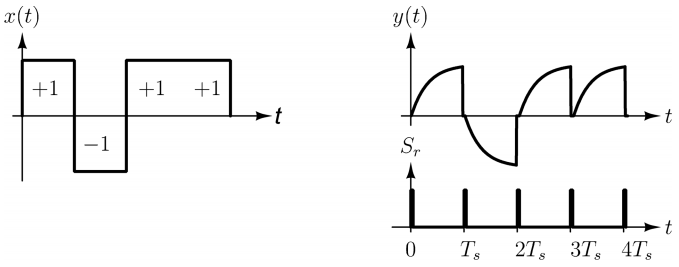

Fig. 9. Symbols transmitted through a channel with reset just after sampling.

As the symbol rate is increased, $T_w = T_s$ decreases, and so does the received signal amplitude (Fig. 4). The noise at the receiver sampling instant changes as well. To analyze the output noise of this system, imagine that symbols are transmitted with a period $T_s = T_w$ as shown in Fig. 9. The output is sampled periodically at $t = nT_s$, and the system is reset just after that. S_R is the signal used to reset the filter. Instantaneous reset is assumed. For the noise n_{ch}, this is a linear periodically time-varying (LPTV) system with a period T_s. The spectral density of the cyclostationary noise at y can be rigorously analyzed using LPTV theory [14]. Here we give only an intuitive explanation. With a filter which is not reset, i.e., the conventional LTI filter, the noise variance would be

$$\sigma_{n,0}^2 = N_0 \int_0^\infty |H_R(f)|^2 \, df = \frac{N_0}{2} \int_0^\infty h_R^2(t) dt \qquad (3)$$

where N_0 is the one-sided spectral density of white noise n_{ch}. When the filter's state variables are periodically reset, it can be worked out that the noise variance just before reset is

$$\sigma_{n,rst}^2 = \frac{N_0}{2} \int_0^{T_s} h_R^2(t) dt \qquad (4)$$

This makes intuitive sense because noise builds up for a duration of T_s between successive state-variable resets. Clearly (4) is smaller than (3) and approaches the latter as T_s is increased. This is an important distinction between the case with and without reset. With reset, as T_s decreases (data rate increases), the noise variance decreases. This partially compensates for the reduction in signal amplitude as the data rate is increased because $T_w = T_s$ decreases.

Fig. 10 compares the performance of state-variable reset with other alternatives for increasing the data rate. Fig. 10(a) and (b) show the received signal amplitude and resulting *SNR* for the three cases. These are normalized to the "conventional" 1 b/s signaling case. For multi-level signaling, the minimum amplitude is considered. The received signal amplitude remains constant with data rate for equalization, but reduces for the other two cases. *SNR* degrades as data rate is increased for all schemes, but state-variable reset has a better *SNR* than the other two. Fig. 10 shows efficiency measures, i.e., *SNR* normalized to the average transmit power P_{TX} or the average transmit energy per bit $E_{TX,b}$ (= P_{TX} divided by the data rate). In this particular example, P_{TX} is constant because the transmitter voltage ± 1 V is applied across $R_{in} = 1\ \ \Omega$ in all cases. For the first-order channel in Fig. 2 Conventional 1 b/s signaling case is again the baseline for comparison. It is seen that state-variable reset also has better

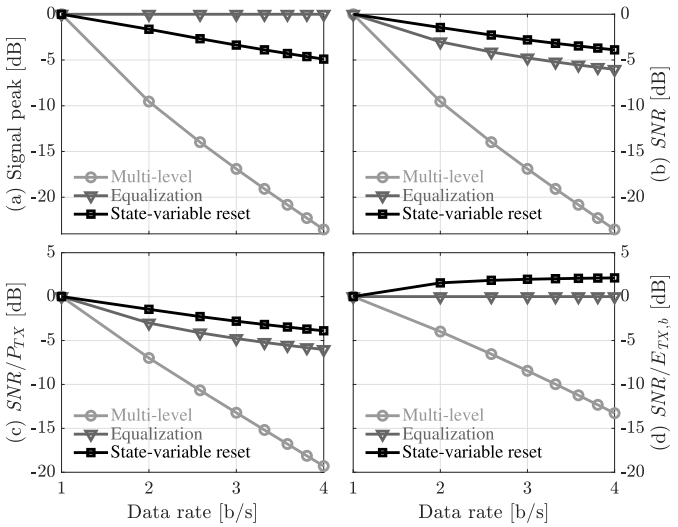

Fig. 10. *SNR* and efficiency of different alternatives for increasing the data rate through the first-order channel in Fig. 2. All numbers are normalized to conventional 1 b/s case.

TABLE I
SIGNAL AND NOISE VALUES IN FIG. 10

Rate (b/s)	Technique	Minimum signal voltage	Mean-sq. noise	Average power	Parameter
1	Conventional	1	$\sigma_{n,0}^2$	1	
M	Multi-level	$\frac{1}{N-1}$	$\sigma_{n,0}^2$	$\frac{N+1}{3(N-1)}$	$N = 2^M$
	Equalization	1	$M\sigma_{n,0}^2$	1	
	State-var. reset	$1 - e^{-\pi T_w}$	$\left(1 - e^{-2\pi T_w}\right)\sigma_{n,0}^2$	1	$T_w = 1/M$

efficiency than the other two. In this comparison, additional power consumption required in the circuit implementation of the equalizer, the multi-level transmitter and receiver, or state-variable reset is not considered. It has to be mentioned here that the proposed technique for increasing the data rate is applicable only in those situations where the state variables of the channel are accessible for reset while multi-level signaling and equalization can be used with any bandlimited communication channel. The quantities plotted in Fig. 10 can be obtained by simulating (in a circuit or system simulator) the linear channel with a single pulse input and determining the sampled output, integrated output noise, as well as current driven into the input resistance of the channel. For the first-order case, the quantities can also be computed symbolically and are given in Table I.

IV. INDUCTIVELY COUPLED CHIP-TO-CHIP LINK

A. Link Model

Fig. 11 shows an inductively coupled link. Two coils L_1 and L_2 with a coupling coefficient k between them communicate through magnetic coupling. They have loss resistances R_1 and R_2 respectively. The two sides are resonated using capacitors C_1 and C_2 respectively. The "noise" source is the magnetic field interference B_n which induces a current in the receive coil. Assuming identical resonances ($L_1 = L_2 = L, R_1 = R_2 = R$ and $C_1 = C_2 = C$) for simplicity and $k \ll 1$ the

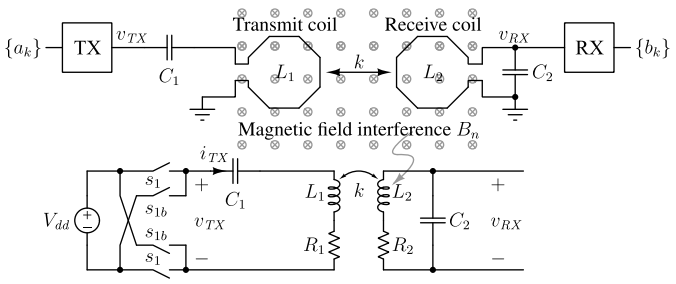

Fig. 11. Inductively coupled link with magnetic field interference.

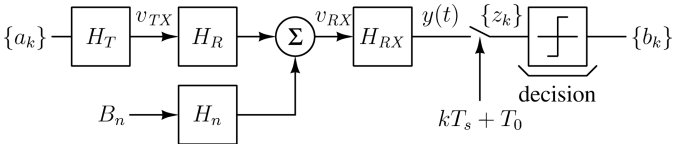

Fig. 12. Model of the inductively coupled link in Fig. 11. H_R and H_n are given in (5).

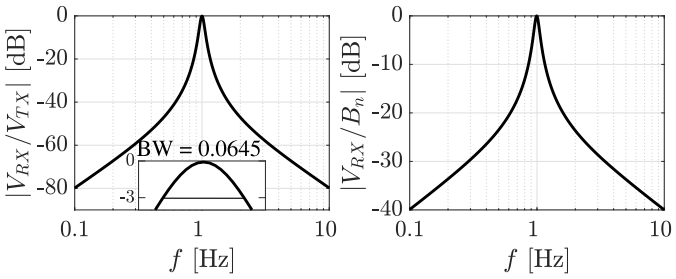

Fig. 13. Magnitude responses of H_R and normalized H_n.

transfer functions are given in the expressions below.

$$H_R = \frac{V_{RX}}{V_{TX}} = kQ^2 H_{bp2}^2$$
$$H_n = \frac{V_{RX}}{B_n} = A_2 \omega_0 Q H_{bp2} \tag{5}$$

where H_{bp2} is the second-order transfer function

$$H_{bp2}(s) = \frac{s/Q\omega_o}{s^2/\omega_o^2 + s/Q\omega_o + 1}. \tag{6}$$

$\omega_o = 1/\sqrt{LC}$ and $Q = \sqrt{L/C}/R$. As expected, with weak coupling, the channel behaves as a cascade of primary and secondary band-pass filters [15]. At the resonance frequency $s = j\omega_o$, the link transfer function is kQ^2. The transfer function from B_n to V_{RX} is a second-order band-pass filter. A_2 is the area of L_2. If L_2 consists of multiple loops, the effective area is the algebraic sum of areas of individual loops. In the following discussions, when Q is varied, it is assumed that L and C are fixed and R is varied. Fig. 12 shows the model of the inductively coupled link from a_k to $y(t)$. H_T is the transmit pulse-shaping filter which could include equalization. H_{RX} is the receiver equalization filter if used.

B. Data Rate Without State-Variable Reset

In the following discussions, we use $L = 1/2\pi$ H, $k = 0.01$, $C = 1/2\pi$ F, and $Q = 10$ ($R = 0.1\ \Omega$). This results in a link with a gain $kQ^2 = 1$ at the center frequency of 1 Hz. Fig. 13 shows the magnitude responses of H_R and H_n. The latter is normalized to a peak of 0 dB. H_R has a

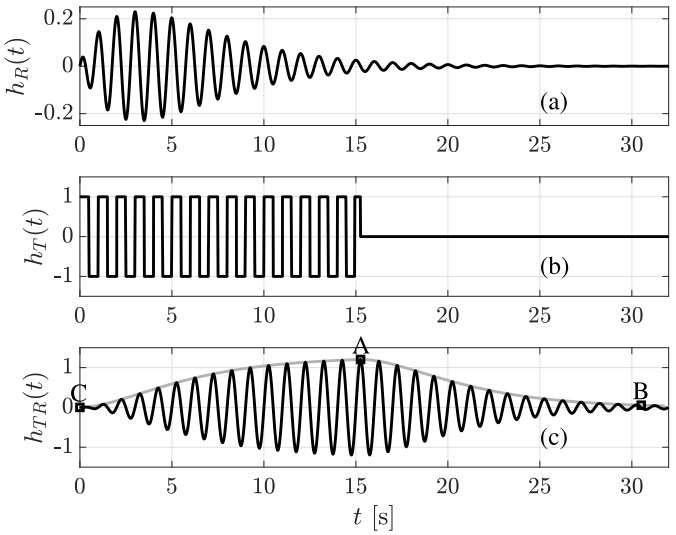

Fig. 14. (a) $h_R(t)$ of the inductively coupled link, (b) Binary matched pulse $h_T(t)$ with a width $T_w = 15.5$, (c) Corresponding $h_{TR}(t)$.

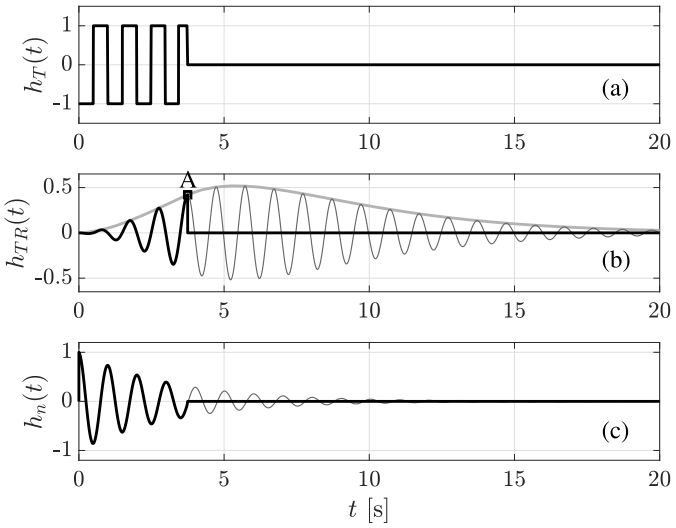

Fig. 15. (a) Binary matched pulse $h_T(t)$ with $T_w = 3.75$, (b) Corresponding $h_{TR}(t)$, (c) $h_n(t)$, normalized to its peak of 6.22×10^{-3}; Thin lines in (b, c) are without reset.

bandwidth of 0.0645 Hz. Fig. 14(a) shows the channel impulse response $h_R(t)$ corresponding to $H_R = V_{RX}/V_{TX}$. It consists of sinusoidal oscillations which build up and die out as expected from a cascade of two high-Q band-pass filters. The Nyquist signaling rate for a 0.0645 Hz band-pass bandwidth is 0.0645 b/s. Fig. 14(b) shows the binary matched pulse from (1) with a width $T_w \approx 1/0.0645$. As expected, the binary matched pulse is nearly a square wave at 1 Hz limited to a width T_w. Fig. 14(c) shows the response $h_{TR} = h_T * h_R$. A band-pass signal such as this one needs to be demodulated. An ideal peak detector is assumed. Its output is shown using a gray line in Fig. 14(c). The peak is at "A" ($\approx 4/\pi$ because the input is a ± 1 square wave) and the ISI at "B" which is one-bit interval away is 27 dB below the peak, again deemed negligible.

C. Data Rate With State-Variable Reset

We attempt to increase the data rate by four times by resetting the state variables. Fig. 15(a) shows h_T which is

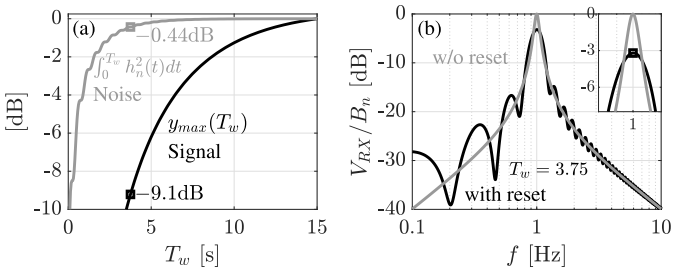

Fig. 16. (a) Change in received signal and noise with T_w, (b) Effect of reset on sinusoidal interference B_n for $T_w = 3.75$.

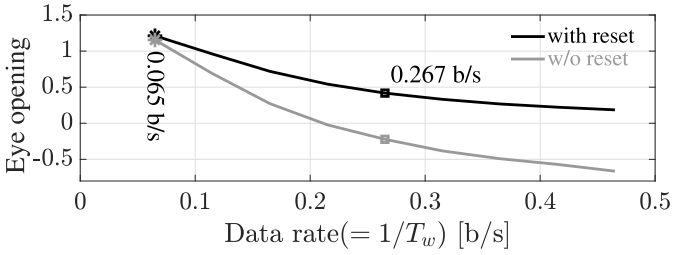

Fig. 17. Eye-opening versus data rate with and without state-variable reset. Negative values imply complete eye closure.

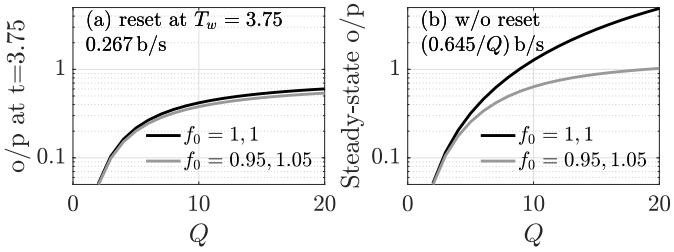

Fig. 18. Effect of resonance frequency mismatch and Q variation. (a) With reset at $T_w = 3.75$, (b) Steady-state output without reset.

binary matched to h_R for $T_w \approx 3.75$ and Fig. 15(b) shows the response to it. It is assumed that the state variables (inductor currents and capacitor voltages in Fig. 11) are reset at $t = 3.75$. The response with reset is shown with a thick line and the response without reset with a thin line. Assuming that resetting is accomplished, we can use a bit rate of $1/3.75 = 0.267$b/s, which is four times the Nyquist rate for this channel. Comparing Fig. 15(b) with Fig. 14(c), we can see that the cursor amplitude is 0.42 in the former and 1.21 in the latter. State-variable reset, therefore, has a penalty of 9.1 dB in the received signal peak. Fig. 16(a) shows the change in the signal peak and noise (given by 4) with T_w. These are normalized to the values obtained for conventional signaling without state-variable reset, i.e., $T_w = 1/0.0645$. For the chosen $T_w = 3.75$, noise is lower by 0.44 dB and the *SNR* penalty is 8.66 dB. The signal energy reduces a lot more rapidly than noise as T_w decreases. This is because the amplitude of oscillations in h_n falls monotonically (Fig. 15(c)) whereas that in h_R rises and falls (Fig. 15(b)). It is easily seen that the part of h_n shown with a thick line in Fig. 15(c) contains most of the total energy in h_n, but the part of h_R shown with a thick line in Fig. 15(b) contains a much smaller fraction of the total energy of h_R. Nonetheless, increasing the data rate using state-variable reset will be shown to be more efficient than the other alternatives. In the above discussions, noise is assumed to be white. Resetting the state variables also changes the effect of narrow-band interference. Fig. 16(b) compares the gain $|V_{RX}/B_n|$ for sinusoidal interference with and without reset. For the case without reset, this is simply the magnitude response corresponding to V_{RX}/B_n. For the case with reset, the received value at $t = T_w$ due to a sinusoidal interference $b_n(t) = \cos(2\pi f t + \phi_i)$ is given by the convolution

$$b_n * h_n|_{t=T_w} = \int_0^{T_w} \cos(2\pi f \tau + \phi_i) h_n(T_w - \tau) d\tau \quad (7)$$

The maximum magnitude of this as ϕ_i is varied from 0 to 2π is taken as the resulting interference. This is shown as a function of f in Fig. 16(b). It has nulls at integer multiples of $1/T_w = 0.267$ Hz. When compared to the case without reset, the effect of interference is higher at some frequencies and lower at others. The peak gain at the center frequency $f_0 = 1$ Hz is 3.1 dB lower, but the peak is broader. This means that narrowband interference close to the center frequency will have a smaller effect when state-variable reset is employed. This is because, with state-variable reset, the interval of integration is T_w as given in (7). Without reset, it would be infinity. This is similar to noise in these two cases given by (4) and (3) respectively.

Fig. 17 shows the eye-opening (with an ideal peak detector) versus data rate (assumed equal to $1/T_w$, where T_w is the width of the transmit pulse) for on-off keying with and without state-variable reset. As the data rate is increased from the Nyquist signaling rate of 0.065 b/s, the eye-opening drops more rapidly without state-variable reset because of ISI. Ideally, with state-variable reset, there is no ISI because the response is reset to zero after $t = T_w$.

D. Q Variation and Resonance Frequency Mismatch

In practice, there are variations in Q as well as the resonance frequency. Fig. 18(a) shows the output versus Q (assumed to be the same on both sides) for a binary matched input for the nominal f_0 of 1 Hz when the state variables are reset at $T_w = 3.75$. This corresponds to "A" in Fig. 15(b). Fig. 18(b) shows the steady-state output without reset. This corresponds to "A" in Fig. 14(c). While Fig. 18(b) shows higher peak values for a given Q than Fig. 18(a), the data rate is lower than in the latter. Because of reset, a data rate of 0.267 b/s is possible for every value of Q in Fig. 18(a). The data rate without reset is $(0.645/Q)$ b/s.

The signal peak with reset at $T_w = 3.75$ varies a lot less than the steady-state output as Q is varied. This is because, while the steady-state gain kQ^2 strongly depends on Q, the initial build-up of the output does not. A first-order analogy to this is a transconductor with a dc input driving a resistor and capacitor in parallel. While the steady-state output is proportional to the resistor value, the initial buildup depends mostly on the capacitor.

As for resonance frequency mismatch, the lowest received amplitude turns out to be when the resonance frequencies of the two coils are skewed in opposite directions from the driving signal frequency. The input is a binary matched pulse assuming 1 Hz resonance frequency on both sides. The gray

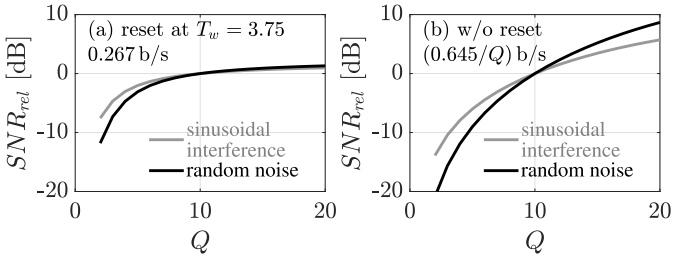

Fig. 19. *SNR* variation with Q: (a) With reset at $T_w = 3.75$, (b) Steady-state operation without reset.

lines in Fig. 18(a) and (b) show the respective outputs. The signal peak with reset at $T_w = 3.75$ varies a lot less than the steady-state output with resonance frequency mismatch. This is again because the steady state gain strongly depends on the two resonance frequencies, but the initial build-up of the output does not. Steady-state operation with high Q on both sides demands more accurate tuning than the proposed state-variable reset technique. For low Q, even the steady-state output is not sensitive to resonance frequency mismatch. This is to be expected because the resonances are broad and skewing them does not significantly lower the gain at the center frequency. Fig. 19 shows the *SNR* variation with Q, normalized to the value at $Q = 10$, with and without reset. The black and gray lines correspond to broadband noise and sinusoidal interference respectively. The lower sensitivity to Q for the case with reset is again seen here. The results shown here are specific to the chosen reset interval $T_w = 3.75$, i.e. reset after four pulses. If the two sides are reset after more pulses, the flattening of *SNR* occurs at a higher Q.

In practice, it is beneficial to operate with the highest possible Q and state-variable reset. While *SNR* due to external field B_n is insensitive to Q, the slightly increased received signal amplitude (Fig. 18(a)) helps with internal circuit noise of the receiver which is independent of the Q of the coils.

E. SNR and Efficiency With Increasing Data Rate

As with the first-order channel, data rate can be increased using multi-level signaling, equalization, or simply lowering Q. For multi-level signaling, the variation of *SNR* and efficiency with data rate are the same as in the first-order case. For equalization, a filter $H_{RX} = \left(Q/Q'\right)^2 \left(s^2/\omega_o^2 + s/Q\omega_o + 1\right)^2 / \left(s^2/\omega_o^2 + s/Q'\omega_o + 1\right)^2$, $Q' < Q$, broadens the bandwidth by Q/Q', and increases the data rate in the same proportion. The transfer function for noise is $H_n H_{RX}$, and the integrated noise is $\int |H_n H_{RX}|^2 \, df$, which increases with increasing Q/Q'. Lowering the quality factor Q to $Q' < Q$ on both sides allows Q/Q' times higher data rate with negligible ISI. It also reduces both the signal amplitude and the noise at the sampling instant. It can be shown that *SNR* degrades. Unlike the ideal first-order channel shown in Fig. 2, the input impedance of the inductively coupled link is frequency dependent. The average transmit power has to be calculated by averaging the product of the current driven from the switching transmitter i_{TX} (Fig. 11) and the transmit voltage V_{TX}. As Q is reduced, the current i_{TX} drawn by the primary, and hence the average power, also reduces. Fig. 20

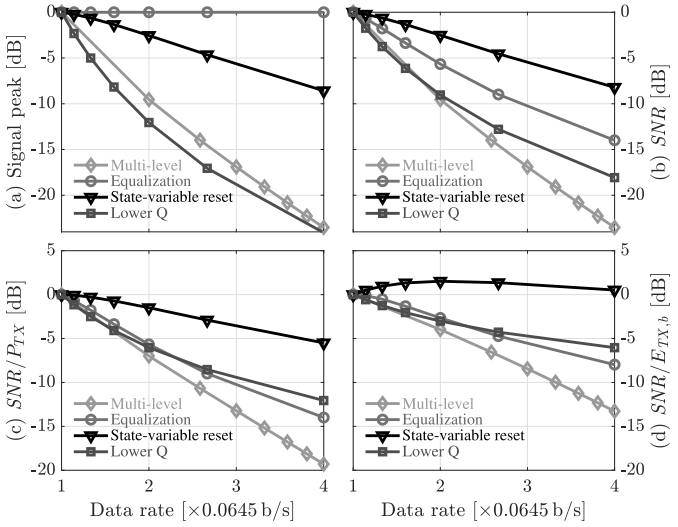

Fig. 20. *SNR* and efficiency of different alternatives for increasing the data rate through the inductively coupled link in Fig. 11. All numbers are normalized to conventional 0.067 b/s case.

shows the change in the received signal amplitude, *SNR*, and efficiency (*SNR* normalized to average transmit power P_{TX} or energy per bit $E_{TX,b}$). The received signal amplitude decreases in all cases except equalization. But, *SNR* degrades the least with state-variable reset. The efficiency measures are also higher with state-variable reset. Therefore, assuming that resetting the state variables is feasible, it is always better to use a higher Q and reset the state-variables than to use a lower Q to allow the response to decay more rapidly. This is similar to the choice made in [16] where, in a high-speed flash ADC, an integrating amplifier with reset is used instead of a wide-band amplifier which settles completely. The former provides a higher gain at lower power consumption.

F. Design Trade-Offs

In order to maximize the data rate, the transmit pulse width T_w has to be minimized. As seen in Fig. 16 reducing T_w significantly reduces the received signal amplitude. This is also seen in Fig. 14(c) and Fig. 15(b) where the amplitude of the first couple of pulses is very small. In practice, this means that, to increase the data rate beyond a certain value, the resonance frequency of the two sides must be increased so that a sufficient number of pulses which results in an acceptable amplitude at the receiver can be used. This is consistent with the conventional inductively coupled link operating in steady state. For a given Q, a higher center frequency implies a higher bandwidth, enabling a higher data rate. The link gain is proportional to the coupling coefficient k. For a given inductor configuration, i.e. face-to-face or coplanar, the area of the inductors has to be increased to increase k. The larger the inductor, the lower its self-resonance frequency. The actual resonance frequency has to be chosen to be lower than this to leave room for trimming. The transmitter and receiver circuits should be capable of operation at the resonance frequency. Thus, the data rate can be limited by the coupled inductor structure or the active circuitry. In cases where isolation is a primary concern, such as the prototype described in this

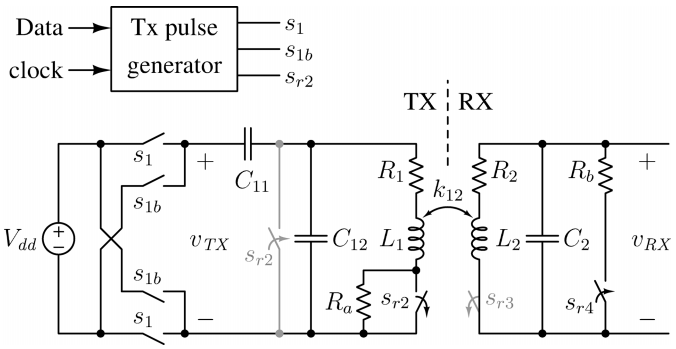

Fig. 21. Implementation of the transmitter and the reset switches on the primary and secondary sides. Switches $s_{R1,3}$ are omitted in the implementation.

paper, the coils would be far from each other, and the coupling coefficient is likely to be small. The inductors have to be large to compensate for this, and their self-resonance frequency limits the data rate. In cases where the coils face each other, the coupling coefficient can be large, and the self-resonance frequency may not be a significant limitation. The proposed technique has a better *SNR* at the receiver compared to other techniques and can be used to increase the data rate, increase the isolation, or reduce the coil size.

V. Prototype System

The principles described above are demonstrated with a chip-to-chip inductively coupled link. The prototype has $Q = 10$ on both sides and $k = 0.01$, same values as in the example in Section IV-A. The transmitter has a 1-turn 6 nH coil and the receiver has a 2-turn 12-nH coil. They are in the same plane on two different chips with their edges $\sim$ 0.5 mm apart. This ensures a high isolation. The center frequency, limited by the self-resonance frequency of the coils, is 2 GHz which yields a bandwidth of 130 MHz. With conventional data transmission, a data rate of about 130 Mb/s can be achieved with negligible ISI.

Fig. 21 shows the inductively coupled link and the switching transmitter. The capacitor on the primary side is split into C_{11} and C_{12}. Each pair of $s_{1,1b}$ is implemented using CMOS inverter drivers. Four switches s_{r1-r4} are required to short circuit two capacitors and open circuit two inductors. From simulations, two switches s_{r2} and s_{r4} are found to be sufficient. This scheme avoids a switch s_{r1} in parallel with the primary coil which experiences large voltage swings and a switch s_{r3} in series with the secondary coil which degrades Q. Resistors R_a and R_b are added to mitigate the effects of switching transients and charge injection. A pulse generator circuit is used on the transmit side to generate s_1, s_{1b}, and s_{r2}. On the receiver side, the tank has to be reset after the bit is successfully detected. To avoid clock and data recovery circuits, on-off keying with transition encoding is used. The generation of reset in the receiver is discussed later in this section.

Fig. 14 shows an idealized realization with instantaneous reset after $T_w = 3.75$, the duration of the first four pulses of h_R. The system can be operated with $T_s = T_w = 3.75$. In the implementation, the following changes are made. The transmitter is based on a reference at 2 GHz, the same as the center frequency of the inductively coupled link. The bit period

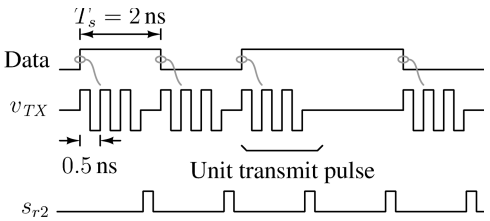

Fig. 22. Transition coding used in the transmitter.

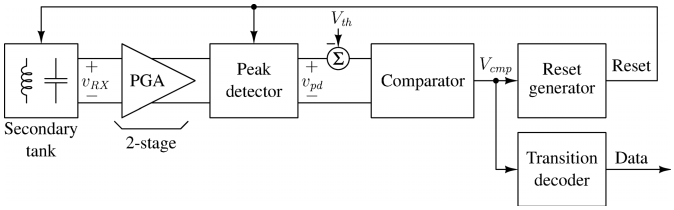

Fig. 23. Receiver block diagram.

is set to four cycles at this frequency, or 2 ns, yielding a data rate of 500 Mb/s. The transmitter and receiver require about 300 ps for reset. Therefore, only three pulses are used in the transmitter, and the remaining cycle (500 ps) is used for reset. Also, as seen in Fig. 14, the half cycles of h_R are of unequal width, ranging from $0.46/f_0$ to $0.5/f_0$. For convenience, the transmitter uses half cycles of equal width $0.5/f_0$. This causes a slight deviation from the condition in (1) and a slight reduction in the received signal strength. Fig. 22 shows the transition encoded transmit signal. A unit pulse is transmitted whenever there is a data transition.

Fig. 23 shows the block diagram of the receiver. The secondary tank voltage V_{RX} drives a programmable gain amplifier (PGA). A peak detector demodulates the PGA output and drives a comparator. V_{th} is the threshold voltage for decisions between on and off levels. This threshold is implemented as a dc bias in the pseudo-differential output of the peak detector. The transmitted data is recovered by toggling the output stream whenever the comparator output has a high-going pulse. After a certain delay following the pulse, the secondary tank and the peak detector are reset. The reset is released after holding it down for an interval sufficient to clear the memory in the tank and the peak detector. The reset should not happen too soon, i.e., well within the bit interval. In this case, the peak-detector output may build up to a value which is high enough to trigger the comparator once more within the same bit interval. The reset delay should not be very long either, since, in that case, another bit interval may have begun before the reset occurs, and a bit maybe missed completely. This is because the transmitter is not aware of the timing in the receiver. The PGA gain, peak detector time constant, and the reset path delay have to be chosen appropriately to avoid this situation. The PGA provides a gain programmable from 9 dB to 29 dB at 2 GHz to compensate for variations in PVT and the mounting distance between the transmitter and receiver chips. The reset delay and width are adjusted to avoid premature or delayed reset over PVT variations. This scheme has the simplicity of resetting the receiver without a full-fledged clock and data recovery circuit.

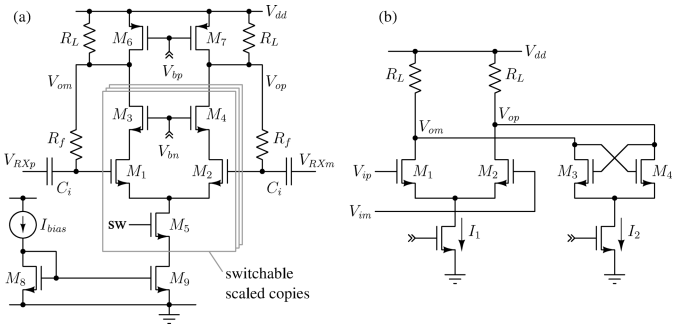

Fig. 24. (a) Each stage of the two-stage PGA, (b) Comparator.

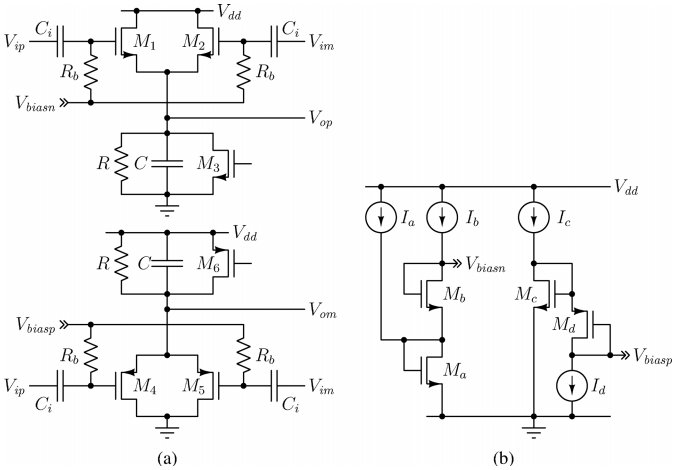

Fig. 25. (a) Peak detector, (b) Biasing circuit.

The PGA is realized as a cascade of two stages. Each stage is shown in Fig. 24(a). It is a differential amplifier with input ac coupling and low-frequency negative feedback through R_f to reduce the output offset. Cascode transistors $M_{3,4}$ are used to reduce Miller effect and increase isolation between the PGA output and the secondary tank. pMOS current sources $M_{6,7}$ are used in parallel with load resistors R_L to increase the gain. Using resistive loads eliminates the need for common mode feedback. Gain is made programmable by (a) Switching in one or more scaled input differential pair units (M_{1-4} using switch M_5)—Three units are used in the first stage and two in the second, and (b) Varying R_L and I_{bias} in discrete steps.

The peak detector is shown in Fig. 25. The nMOS pair $M_{1,2}$ detects the positive peaks of differential inputs V_{ip} and V_{im}. The pMOS pair $M_{4,5}$ detects the negative peaks of V_{ip} and V_{im}. The gain is maximized by using both of the differential inputs V_{ip} and V_{im}, and detecting both positive and negative peaks. Switches $M_{3,6}$ reset the peak detectors. Because the nonlinearity of the MOS transistor is mild, the gain (ratio of the dc output to the peak of the 2 GHz input sinusoid) is about 0.5. The difference between the dc bias of $V_{op} - V_{om}$ is required to be equal to $-V_{th}$, where V_{th} is the desired comparator threshold (Fig. 23). A problem with this peak detector is that the bias voltages at V_{op} and V_{om} are shifted in different directions from the input bias. The amount of shift is highly dependent on process and temperature. To mitigate this problem, the peak detector is ac coupled to the PGA output. The dc bias voltages V_{biasn} and V_{biasp} are generated

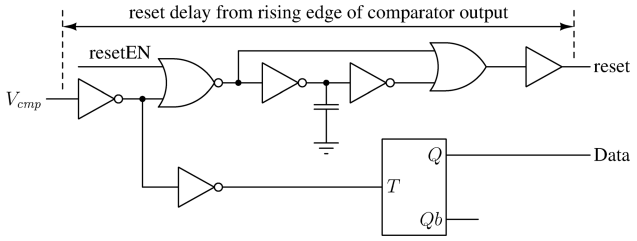

Fig. 26. Transition decoder and reset generator.

as shown in Fig. 25(b). The bias voltages are referred to the lower rail and are independent of the supply voltage. M_c is biased near the subthreshold region. The threshold voltage dependent terms in the output $V_{op} - V_{om}$ cancel out, largely eliminating dependence on the process and temperature. The resulting output dc bias is dependent on the sum of nMOS threshold voltages. This is set to $-V_{th}$, the desired threshold of the comparator, by adjusting the currents and sizes suitably. Simulations show that the dc offset in the output $V_{op} - V_{om}$ varies by about 30 mV over PVT variations. This is sufficiently small for robust detection by the comparator.

Fig. 24(b) shows the comparator. The ratio of sizes of $M_{3,4}$ to $M_{1,2}$ and I_2 to I_1 are set to obtain a hysteresis of 60 mV. The buffered output of the comparator drives a transition flip-flop to recover the transmitted data as shown in Fig. 26. The comparator output and its delayed version are combined to generate a reset for the secondary tank and the peak detector.

VI. Comparison With Other Techniques

A number of techniques have been published in the literature for increasing the data rate through an inductively coupled link. [3] demonstrates a 2.5 Mbps FSK transmission over an inductively coupled link tuned to 7 MHz center frequency. The link has a series and a parallel resonant circuit on the primary side and a parallel resonant circuit on the secondary side. The quality factors of the resonances, calculated individually, are < 2.5. If a higher Q is used to increase the gain, the link becomes slower. The links in [4] and [5] use a form of equalization to truncate the impulse response of an inductively coupled link. It works perfectly only for a second order system (poles at $-\sigma \pm j\omega$) whose impulse response is of the form $\exp(-\sigma t)\sin(\omega t)$. If a delayed, scaled version of such a response is added to itself, it is possible to cancel the response beyond the delay period. The inductively coupled link has a fourth order response. When one of the sides has a very small Q, the response is approximately second order corresponding to the higher Q. Due to its approximate nature, the response still exhibits considerable ISI. The transmit pulses used must have a precisely controlled amplitude relationship that depends on σ and timing that depends on ω. Also, because of the low Q on one of the sides which reduces the channel gain, and due to the excitation being a narrow pulse, the received symbol energy is smaller than in the proposed technique. [11] uses a technique called "direct antenna modulation" to remove the persistent sinusoidal response across the primary tank. In contrast to the proposed technique where the primary inductor current is reset to zero after every symbol, in [11], the primary inductor current is held at the value

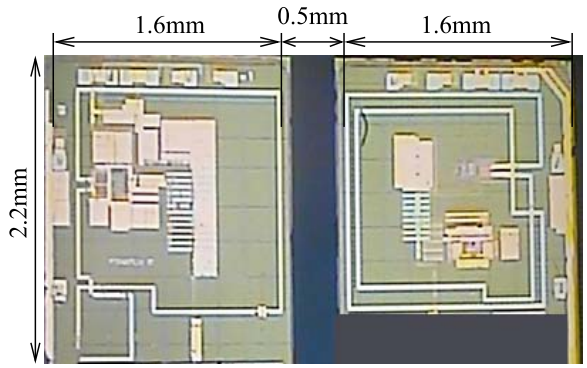

Fig. 27. Chip photograph. Left: Tx, right: Rx. Coil centers are 1.8 mm apart.

present at the end of the symbol by closing the loop around the inductor alone. This reduces the voltage induced on the secondary, Mdi_1/dt, to zero. While this solves the problem of a long impulse response of the high-Q tank on the primary side, a high-Q secondary would still produce a large ISI. In [11], a very low Q secondary is used, which reduces the channel gain. Additionally, the transmit signal needs to be a shaped sinusoid which is more difficult to generate. Also, [11] demonstrates the link only with an alternating bit pattern. Random data produces more complicated ISI patterns, degrading the link performance. In [20] and [21], a high Q resonant network with a variable capacitor is used to match the instantaneous resonance frequency to the two FSK frequencies according to the transmitted data. The amplitude of both FSK tones then correspond to the resonance peak. This would be impossible with a fixed resonant network. Both [20] and [21] demonstrate only a transmitter. The same technique cannot be used straightforwardly in the receiver with a high Q resonant network. This is because, the timing of the capacitor switching has to be derived from the received signal. Therefore, the receiver has to have a low Q, reducing the channel gain.

The key differences of our system compared to the above are (a) both transmitter and receiver Q are maintained at their highest possible value, maximizing the link gain, (b) Transmit signal is chosen to provide the largest possible signal at the end of the symbol period, (c) The transmit signal can be generated using a high-efficiency switching transmitter, (d) reset for the receiver side can be easily generated with on/off keying, and (e) The long channel memory resulting from high Q is cleared after each symbol to prepare the system for the next symbol. Thus high-speed transmission can be achieved with a high power efficiency.

The proposed technique turns a linear time-invariant resonant inductively coupled link into a linear time-varying system by periodically resetting it. The Q of the tank is alternated between its maximum possible value (during signal build up) and zero (at the end of each period). Reference [17] also uses a time-varying network and Q factor modulation, but for a different purpose.

VII. Measurement Results

The transmit driver (Fig. 21) and the receiver (Fig. 23) are implemented in a 0.18μm CMOS process. Fig. 27 shows the chip photograph. Fig. 28 shows the test setup. Data and control are fed to the transmit driver. Received data is captured by a computer for error rate measurements and also monitored on an oscilloscope to obtain the eye diagrams. Because the substrate resistivity was significantly lower than what was modeled and interaction with mandatory metal scribe lines which had to be placed around the die (close to the coils), the lead frame, and the board, the quality factor on each side was only about 7 instead of the intended value of 10. This raises the bandwidth to 185 MHz. As seen in Fig. 18 and 19, the proposed scheme is not very sensitive to Q.

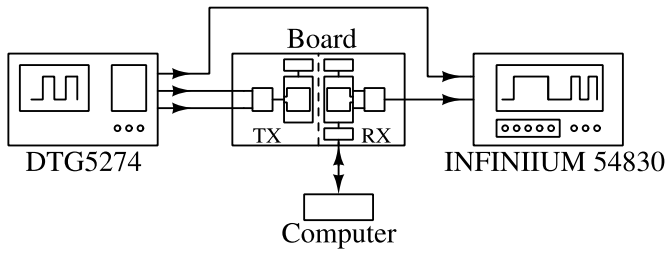

Fig. 28. Test setup.

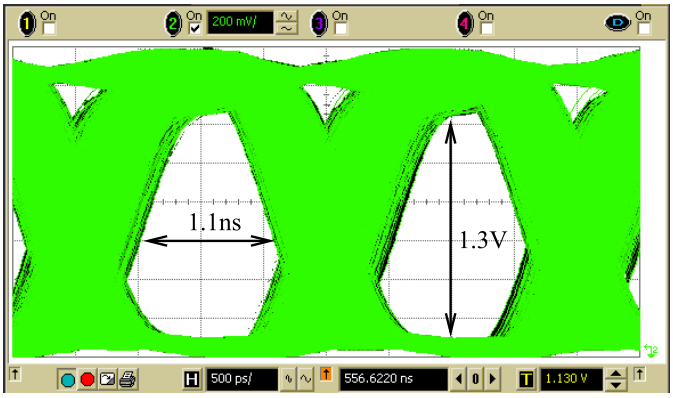

Fig. 29. Measured eye diagram at 500 Mb/s with state-variable reset.

Fig. 29 shows the measured eye diagram (at the output of the transition flip-flop in Fig. 26) at 500 Mb/s with state-variable reset enabled. Usually, eye diagrams are measured before the decision-making latch. The vertical and horizontal eye-openings in such an eye diagram convey the signal to noise and signal-to-jitter ratios at the decision point. On this chip, the output of the peak detector was not accessible. Since the decision is made using a transition flip flop, the horizontal eye-opening is nearly the same as at the input of the flip-flop. At 500 Mb/s, the horizontal eye-opening is about 1 ns in the middle of the eye. This indicates that error-free transmission at this rate should be possible. Fig. 30 shows the bathtub curves for the receiver with and without state-variable reset at 300Mb/s. These are measured by feeding the receiver output data (Fig. 26) and a clock which can be phase shifted to a bit error rate tester. The measurement equipment restricted us to 300 Mb/s. The gaps in the middle indicate regions with very low error rate ($< 10^{-12}$, no errors in an hour). Since the tank Q is less than the expected value, conventional on-off keying has some eye-opening at 300 Mb/s. Still, significant improvement is seen when state-variable reset is employed. With state-variable reset, the eye is open for

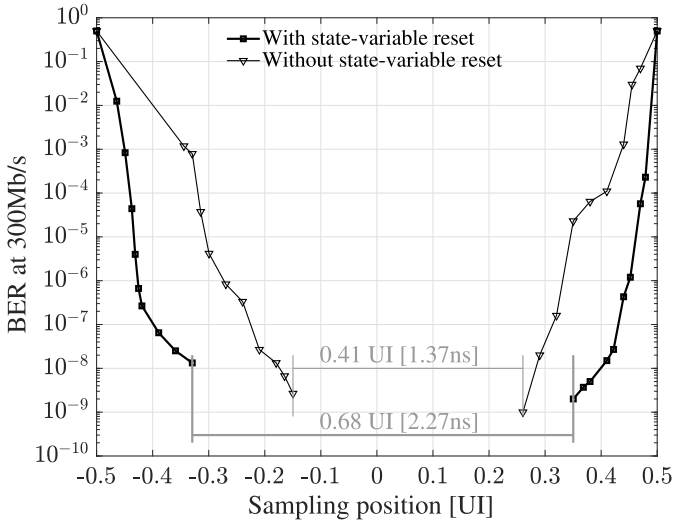

Fig. 30. Measured bathtub at 300 Mb/s with and without state-variable reset.

TABLE II
PERFORMANCE SUMMARY AND COMPARISON

	[3]	[5]	[4]	[11]	[18]	[19]	**This work**
Tech. (μm)	1.5	0.5	Discrete		40nm	0.35	**0.18**
V_{dd} (V)	5	3.3	—	—	1.1	3, 2	**1.8**
$P_{d,TX}$ (mW)	—	3.52	—	—	0.41		**45**‡
$P_{d,RX}$ (mW)	0.38	3					**18**
Energy/bit†	152	639	—	—	200	650	**126**
Isolation (kV)	—	—	—	—		2.5	**7.5**
CMR (kV/μs)	—	—	—	—	—	35	**50**
Q_1	1	1	2.3	2.5	—	—	**6**
Q_2	1	48	45	2.5			**6**
f_o (MHz)	7	67	33	0.27	35	—	**2000**
BW (MHz)	2.5	1.5	0.73	0.067	—	—	**185**
Data rate (Mb/s)	2.5	10.2	5.2	0.27	2	40	**500**
Coupling coeff.	0.05	0.012	0.012	—	—	—	**0.01**
Coil1 dia. (mm)	20	10	10	50	30	—	**1.5**
Coil2 dia. (mm)	12	15	19	50	30	—	**1.5**
Distance (mm)	5	10	10	—	40	—	**1.8**
Arrangement	Facing each other			—	—	—	**In plane**

†: Both Tx and Rx power included where reported; [3] has only an Rx IC.
‡: Different variant of the chip than reported in [9].

2.27 ns and closed for 1.06 ns for BER $< 10^{-9}$. Without reset, the eye is open for 1.37 ns and closed for 1.96 ns. Assuming that the eye closure interval does not change with the data rate, it can be seen that 500 Mb/s operation is not at all possible without state-variable reset, whereas incorporating reset would maintain an open eye for $2 - 1.06 = 0.94$ ns, allowing us to operate comfortably at that rate. This result is consistent with Fig. 29, which visually shows an eye-opening of 1.1 ns at 500 Mb/s. These results clearly show that resetting the state variables enables faster data transmission. The data rate of the prototype is limited by the speed of the peak detector. As for electromagnetic compatibility, the device passed IEC-ED 6100-4-3 level 2 immunity tests and meets CISPR22 class-B emissions standard. For immunity testing, the device is exposed to RF radiation from 80 MHz to 2.7 GHz with 3V/m (Level 2) of field strength at the device under test. Immunity can be further improved if necessary by using figure-eight shaped coils in the receiver and transmitter such that the voltages induced in the two loops due to the transmitter add up and those induced due to a uniform external field cancel out. Table II summarizes the performance of the chip and compares it to other published inductively coupled links. These implementations cannot be directly compared to each other since the application and requirements are different. It is seen that the proposed technique achieves high data rate while maintaining a high isolation and energy efficiency.

VIII. CONCLUSIONS

We have presented an approach for faster data transmission through a bandlimited channel when the channel state variables are accessible. By resetting these state variables, the channel response can be truncated in principle to arbitrarily short intervals. A practical link in which this technique can be implemented is the inductively coupled link. We have demonstrated the effectiveness of the technique by realizing 500 Mb/s data transmission through an inductively coupled band-pass channel with 185 MHz bandwidth. This is substantially higher than the rate possible with a conventional communication link without state-variable reset.

In contrast to other techniques for increasing data rates through such channels, the proposed technique allows high-Q resonances on both sides for maximizing the channel gain and uses a transmit pulse that maximizes the energy in the received signal at the sampling instant. Additionally, as the truncation interval is made shorter, the sampled noise energy reduces, compensating to some extent the reduction in the received signal energy. The transmitted signal has a constant absolute value and only changes polarity, allowing the use of efficient switching transmitters. With these techniques, data can be transmitted at a rate faster than what is implied by the bandwidth of such a system at a low energy consumption per bit.

ACKNOWLEDGEMENTS

The authors thank Shanthi Pavan for technical discussions, Madhusudan Gajanur for layout, and Mahesh Reddy for testing.

REFERENCES

[1] *ADuM120N/ADuM121N 3.0 kV rms, Dual-Channel Digital Isolators, ADuM120N/ADuM121N Datasheet*, Analog Devices, Norwood, MA, USA, Jan. 2016.
[2] *IL600A Series Isolators IL600A Datasheet*, NVE, Eden Prairie, MN, USA, Nov. 2013
[3] M. Ghovanloo and K. Najafi, "A wideband frequency-shift keying wireless link for inductively powered biomedical implants," *IEEE Trans. Circuits Syst. I, Reg. Papers*, vol. 51, no. 12, pp. 2374–2383, Dec. 2004.
[4] F. Inanlou and M. Ghovanloo, "Wideband near-field data transmission using pulse harmonic modulation," *IEEE Trans. Circuits Syst. I, Reg. Papers*, vol. 58, no. 1, pp. 186–195, Jan. 2011.
[5] F. Inanlou, M. Kiani, and M. Ghovanloo, "A 10.2 Mbps pulse harmonic modulation based transceiver for implantable medical devices," *IEEE J. Solid-State Circuits*, vol. 46, no. 6, pp. 1296–1306, Jun. 2011.
[6] H. Ishikuro and T. Kuroda, "Wireless proximity interfaces with a pulse-based inductive coupling technique," *IEEE Commun. Mag.*, vol. 48, no. 10, pp. 192–199, Oct. 2010.
[7] N. Miura, M. Saito, and T. Kuroda, "A 1 TB/s 1 pJ/b 6.4 mm^2/TB/s QDR inductive-coupling interface between 65-nm CMOS logic and emulated 100-nm DRAM," *IEEE J. Emerg. Sel. Topics Circuits Syst.*, vol. 2, no. 2, pp. 249–256, Jun. 2012.
[8] Y. Take, N. Miura, and T. Kuroda, "A 30 Gb/s/Link 2.2 Tb/s/mm^2 inductively-coupled injection-locking CDR for high-speed DRAM interface," *IEEE J. Solid-State Circuits*, vol. 46, no. 11, pp. 2552–2559, Nov. 2011.

[9] S. Mukherjee *et al.*, "A 500 Mb/s, 200 pJ/bit die-to-die bidirectional link with 24 kV surge isolation and 50 kV/s CMR using resonant inductive coupling in 180 nm CMOS," in *IEEE Int. Solid-State Circuits Conf. (ISSCC) Dig. Tech. Papers*, 2017, pp. 434–435.
[10] S. Mukherjee, A. Bhat, and K. A. Shrivastava, "Periodic bandwidth widening for inductive coupled communications," U.S. Patent 9 385 790 B1, Jan. 5, 2015.
[11] U. Azad and Y. E. Wang, "Direct antenna modulation (DAM) for enhanced capacity performance of near-field communication (NFC) link," *IEEE Trans. Circuits Syst. I, Reg. Papers*, vol. 61, no. 3, pp. 902–910, Mar. 2014.
[12] S. Pavan. *EE5323: Advanced Electrical Networks*. Accessed: Mar. 1, 2019. [Online]. Available: http://www.ee.iitm.ac.in/vlsi/courses/ee5323/start
[13] J. G. Proakis and M. Salehi, *Digital Communication*, 5th ed. New York, NY, USA: McGraw-Hill, 2008, pp. 178–182.
[14] S. Pavan and R. S. Rajan, "Interreciprocity in linear periodically time-varying networks with sampled outputs," *IEEE Trans. Circuits Syst. II, Exp. Briefs*, vol. 61, no. 9, pp. 686–690, Sep. 2014.
[15] U. Azad, H. C. Jing, and Y. E. Wang, "Link budget and capacity performance of inductively coupled resonant loops," *IEEE Trans. Antennas Propag.*, vol. 60, no. 5, pp. 2453–2461, May 2012.
[16] K. Nagaraj *et al.*, "A dual-mode 700-M samples/s 6-bit 200-M samples/s7-bit A/D converter in a 0.25-μm digital CMOS process," *IEEE J. Solid-State Circuits*, vol. 35, no. 12, pp. 1760–1768, Dec. 2000.
[17] M. Kiani, B. Lee, P. Yeon, and M. Ghovanloo, "A Q-modulation technique for efficient inductive power transmission," *IEEE J. Solid-State Circuits*, vol. 50, no. 12, pp. 2839–2848, Dec. 2015.
[18] A. Yousefi, D. Yang, A. A. Abidi, and D. Markovic, "A distance-immune low-power 4-Mbps inductively-coupled bidirectional data link," in *Proc. IEEE Symp. VLSI Circuits*, Jun. 2017, pp. C60–C61.
[19] S. Kaeriyama, S. Uchida, M. Furumiya, M. Okada, and M. Mizuno, "A 2.5 kV isolation 35 kV/us CMR 250 Mbps 0.13 mA/Mbps digital isolator in standard CMOS with an on-chip small transformer," *IEEE Symp. VLSI Circuits*, Jun. 2010, pp. 197–198.
[20] M. Salehi, M. Manteghi, S.-Y. Suh, S. Sajuyigbe, and H. G. Skinner, "A wideband frequency-shift keying modulation technique using transient state of a small antenna," *Prog. Electromagn. Res.*, vol. 143, pp. 421–445, Dec. 2013.
[21] H. Kennedy, R. Bodnar, T. Lee, and W. Redman-White, "A high-Q resonant inductive link transmit modulator/driver for enhanced power and FSK/PSK data transfer using adaptive-predictive phase-continuous switching fractional-capacitance Tuning," in *IEEE Int. Solid-State Circuits Conf. (ISSCC) Dig. Tech. Papers*, Feb. 2019, pp. 444–446.

Nagendra Krishnapura (M'98) received the B.Tech. degree from IIT Madras, India, and the Ph.D. degree from Columbia University, New York. He was an Analog Design Engineer with Texas Instruments, Bell Laboratories, Celight, Inc., Multilink, and Vitesse Semiconductor. He has taught analog circuit design courses at Columbia University as an Adjunct Faculty. He is currently a Professor with IIT Madras. His interests are analog and RF circuit design and analog signal processing.

Anoop Narayan Bhat received the B.E. degree from the R. V. College of Engineering, Bengaluru, India, in 2012, and the M.S. degree in electrical engineering from IIT Madras, Chennai, India, in 2016. He is currently pursuing the Ph.D. degree with the University of Twente, Enschede, The Netherlands. He was a Design Engineer with Texas Instruments India Ltd., Bengaluru, from 2015 to 2017.

Subhashish Mukherjee received the Master's degree in electrical engineering from IIT Kanpur, Kanpur, India, in 1990. He joined Texas Instruments India Pvt. Ltd., that year and since then, has worked on various data-converter, wire-line (DSL and Cable modem), wireless signal chain, and RF (WLAN, Bluetooth, NFC, and GPS) designs. He has worked on significant technology developments like efficient radio architectures, RF Power Amplifier integration in CMOS, ultra-low power BLE RF, multi-radio coexistence methodology development, high speed, and low power isolation technology development. His current focus is on high-performance frequency synthesizers and wideband mixers.

Kumar Anurag Shrivastava received the Bachelor's degree in electronics and telecommunications from NIT Raipur in 2011 and the Master's degree in VLSI design from IIT Delhi in 2013. He is currently a Lead Design Engineer with Texas Instruments India Pvt. Ltd. His interests include isolators, low power RF circuits, and oscillators.

Madhulatha Bonu received the B.E. degree (Hons.) from BITS Pilani, India, and the M.S. degree from Oregon State University, Corvallis, USA. From 2002 to 2012, she was an Employee of National Semiconductor Corporation. From 2012 to 2017, she was with Kilby Labs, Texas Instruments, working on various chips for isolated die-to-die communication, low power wake up transceivers, and asynchronous ADCs. She has been with Texas Instruments India Pvt. Ltd., since 2012. She is currently with the Low power Audio and Actuators Group (LPAA), working on class-D smart amplifiers.